JOURNAL OF MATERIALS SCIENCE 27 (1992) 6197–6203

Developments in highly toughened CeO_2–Y_2O_3–ZrO_2 ceramic system

J. G. DUH, J. U. WAN
Department of Materials Science and Engineering, National Tsing Hua University, Hsinchu, Taiwan

A wet-chemical approach has been applied to derive fine powders with various ceria and yttria compositions in the CeO_2–Y_2O_3–ZrO_2 ceramic system by the co-precipitation method. The characteristics of the as-derived powders have been evaluated through differential thermal analysis, thermogravimetric analysis, BET surface-area analysis, and inductively coupled plasma technique. The hardness and fracture toughness of the as-sintered specimens were evaluated by the indentation method. A highly toughened ceramic with $K_{IC} > 25$ MPa $m^{1/2}$ was achieved with the composition 5.5 mol% CeO_2–2 mol% $YO_{1.5}$–ZrO_2. The relationship between the mechanical properties and the compositions of stabilizers, CeO_2 and Y_2O_3 is discussed with respect to the degree of tetragonal to monoclinic transformation as well as the grain size of the as-sintered ceramics.

1. Introduction

The investigation of zirconia has continued to attract the interest of a great number of scientists and technologists, and solid evidence of commercial application for the engineering ceramics is now available. To use zirconia to its full potential, the properties of the oxide have been modified by the addition of a cubic stabilizing oxide, particularly MgO, CaO, Y_2O_3 and CeO_2 [1–7]. Tetragonal zirconia polycrystal (TZP) ceramics are attractive because of their excellent room-temperature mechanical properties, wear properties and a thermal expansion coefficient close to that of iron and iron-based alloys [8–12]. The high strength and toughness of TZP is considered to be largely due to the stress-induced martensitic transformation of the metastable tetragonal phase to the stable monoclinic phase. Unfortunately, the fatal disadvantage of yttria-doped Y–TZP occurs at low-temperature ageing in a humid atmosphere [13–17]: mechanical properties decrease with increasing ageing time as a consequence of the spontaneous tetragonal to monoclinic phase transformation.

It has been reported that the ceria-doped Ce–TZP exhibit better thermal stability and higher toughness than Y–TZP [18–20]. However, the strength of Ce–TZP is comparatively low. In order to enhance the strength of Ce–TZP and to improve the thermal stability of Y–TZP at low temperature, Sato *et al.* first reported the availability of Y_2O_3–CeO_2–ZrO_2 ceramics [21]. CeO_2 caused no significant degradation in sinterability and mechanical properties in this system. The stability of the tetragonal phase in Y_2O_3–CeO_2–ZrO_2 ceramics increased with increasing amounts of Y_2O_3 and CeO_2 and with decreasing grain size. Duh *et al.* [20] also showed that partial substitution by Y_2O_3 in CeO_2–ZrO_2 resulted in reduced grain size and tended to stabilize the tetragonal structure. In addition, Y_2O_3 substitution in CeO_2–ZrO_2 increased the hardness, while it decreased the fracture toughness. Hence, it is expected that a optimal composition exists in the Y_2O_3–CeO_2–ZrO_2 system, in which the advantages of individual Y_2O_3–ZrO_2 ceramics and CeO_2–ZrO_2 ceramics are retained and the final product can be used as a promising material with high strength, high toughness and good thermal stability.

This study is the first phase of continuous research in the development of a highly toughened and thermally stable zirconia system. The optimal composition for mechanical properties in the Y_2O_3–CeO_2–ZrO_2 system has been investigated. The powders were fabricated by a co-precipitation method and then characterized by thermal analysis, BET surface measurement and X-ray diffraction. The fracture toughness of the as-sintered specimen was evaluated through an indentation test. The relationship between property, microstructure and fabrication process has been probed and is discussed.

2. Experimental procedure

The powder preparation for this study was based on the coprecipitation method. A similar approach has been reported elsewhere [22]. The previous study [22] dealt with the fabrication of higher CeO_2 contents around 10 mol %. In this study, however, the CeO_2 content was varied from 5–9.5 mol %. $ZrOCl_2 \cdot 8H_2O$, $Y(NO_3)_3 \cdot 5H_2O$ and $Ce(NO_3) \cdot 6H_2O$ were used to prepare the stock solution. The concentrated ammonia solution was dropped into the well-stirred solution in which the pH value was continuously controlled. The stock solution was added to the ammonia solution to form the coprecipitate, which was filtered

0022–2461

by water suction. The filtered coprecipitate was washed at least twice with alcohol, acetone or ethyl ether, following the deionized water wash. The resulting gel was desiccated using an infrared lamp and ground every 5 min until a dry powder was obtained.

The powder was examined by thermogravimetric analysis (TGA) and differential thermal analysis (TG/DTA, Seiko 300). The experiments were carried out to 500 °C with a heating rate of 10 °C min^{-1}. Calcination of the powder was fulfilled at 500 °C for 1 h and followed by wet ball milling for 10–12 h. The wet-milled powder was dried with an infrared lamp. The surface area of as-dried powder was analysed by BET (Micrometrics, ASAP-2000) with helium as the analysis gas. The powders were pressed into pellets in a 1 cm diameter die under various pressures. The green density was about 35% theoretical density. The sintering experiment was carried out in air in an alumina muffle furnace (Linberg, USA) at 1500 °C for 1–8 h.

The bulk density was measured by Archimedes' technique with water as the immersion medium. X-ray phase analysis was performed with an X-ray diffractometer equipped with copper radiation at 30 kV and 20 mA (Rigaku Geigerflex D/MAX-B, Japan). X-ray scans of 2θ between 27 and 33 °C were conducted to estimate the monoclinic to tetragonal ratio. The fraction of monoclinic phase was evaluated from the equation [23]

$$\% \text{ monoclinic} = \frac{I_m(1\,1\,\bar{1}) + I_m(1\,1\,1)}{I_m(1\,1\,\bar{1}) + I_m(1\,1\,1) + I_t(1\,1\,1)} \quad (1)$$

where $I_m(1\,1\,\bar{1})$, $I_m(1\,1\,1)$ and $I_t(1\,1\,1)$ represent the intensity in the monoclinic peaks $(1\,1\,\bar{1})$, $(1\,1\,1)$ and tetragonal peak $(1\,1\,1)$, respectively. In addition, the powder compositions were determined by inductively coupled plasma (ICP, Shimadzu GVM-1000P).

The morphology of the as-sintered specimen surface was examined with a scanning electron microscope (SEM, Cambridge 250 MK3). The average grain size of the samples was estimated by the intercept method. For the indentation test, samples were ground with SiC paper and polished with 6 and 1 μm diamond pastes in sequence to produce an optically reflective surface. The hardness was measured by Vickers' indentation (Matsuzawa MV-1) with a load from 196–490 N. The fracture toughness was calculated from the following equations [24].

(1) Niihara *et al.* [25]

$$\left(\frac{K_{IC}\phi}{Ha^{1/2}}\right)\left(\frac{H}{E\phi}\right)^{2/5} = 0.035\left(\frac{l}{a}\right)^{-1/2} \quad (2)$$

for $0.25 \leq l/a \leq 2.5$,

$$\left(\frac{K_{IC}\phi}{Ha^{1/2}}\right)\left(\frac{H}{E\phi}\right)^{2/5} = 0.129\left(\frac{c}{a}\right)^{-3/2} \quad (3)$$

for $c/a \geq 2.5$

(2) Shetty *et al.* [26]

$$K_{IC} = 0.0319\frac{P}{al^{1/2}} \quad (4)$$

(3) Lankford [27]

$$K_{IC} = 0.0363\left(\frac{E}{H}\right)^{2/5}\left(\frac{P}{a^{1.5}}\right)\left(\frac{a}{c}\right)^{1.56} \quad (5)$$

(4) Lawn *et al.* [28]

$$K_{IC} = 0.0134\left(\frac{E}{H}\right)^{1/2}\left(\frac{P}{c^{3/2}}\right) \quad (6)$$

where K_{IC} is the Mode I critical stress intensity factor, H the hardness, E the Young's modulus, c the radius of the surface crack, a the half-diagonal of the Vickers' indent, P the load on indentor, l a parameter defined as c-a, and ϕ, defined as hardness H to uniaxial yield stress σ_y, is almost a constant ($\phi \approx 2.7$–3).

Low-temperature annealing experiments in water were performed in a sealed stainless holder at 200 °C for various times [22]. The annealed specimens were examined by X-ray diffraction and their mechanical properties were also measured by an indentation method.

3. Results and discussion

3.1. Powder characteristics

The differential thermal analysis (DTA) and thermal-gravimetric analysis (TGA) of dry uncalcined powder for the composition 5.3 mol % CeO_2–2 mol % $YO_{1.5}$–ZrO_2 with different solvents are shown in Fig. 1. In Fig. 1a and b, the exothermic peak of the glow transition [29] is not as sharp as that in Fig. 1c and d. As shown in Fig. 1a and b, DTA curves of alcohol-derived and acetone-derived gels exhibit a similar shape. Nevertheless, the alcohol-derived gel has two obscure peaks at 228 and 317.5°C, respectively, while the acetone-derived gel has only one at 299.6 °C. The peak at 228.0 °C in Fig. 1a may be due to the interaction between CeO_2–$YO_{1.5}$–ZrO_2 gel and the hydroxide functional group in alcohol. In fact, the CeO_2–$YO_{1.5}$–ZrO_2 gel has excellent dispersion in alcohol and acetone. There is a sharp exothermic peak at 440 °C as indicated in Fig. 1c and there is also an obscure peak at 299.6 °C, similar to that in Fig. 1b. As shown in Fig. 1d, there is a sharp exothermic peak at 459 °C and a clear peak at 278.2 °C which is due to the strong hydrogen bond interaction between gel and water. This indicates that the temperature radiated by the infrared lamp on the gel is below 278 °C. The strong and sharp exothermic glow transition peak in Fig. 1c and d implies that mass crystalline transition takes place.

The compositions of the as-synthesized powders were evaluated by the ICP technique. Table I summarizes the compositions of powders employed in this study. The measured compositions are usually less than those in the nominal compositions because the raw materials may absorb humidity and also the coprecipitation reaction is not fully completed. In the case of calibrated compositions, the yttria oxide contents ($YO_{1.5}$) in Series I are normalized to 2.0%, while those in Series II are normalized to 1.5%. The corresponding CeO_2 contents are then proportionally weighted. The purpose of the employment of the

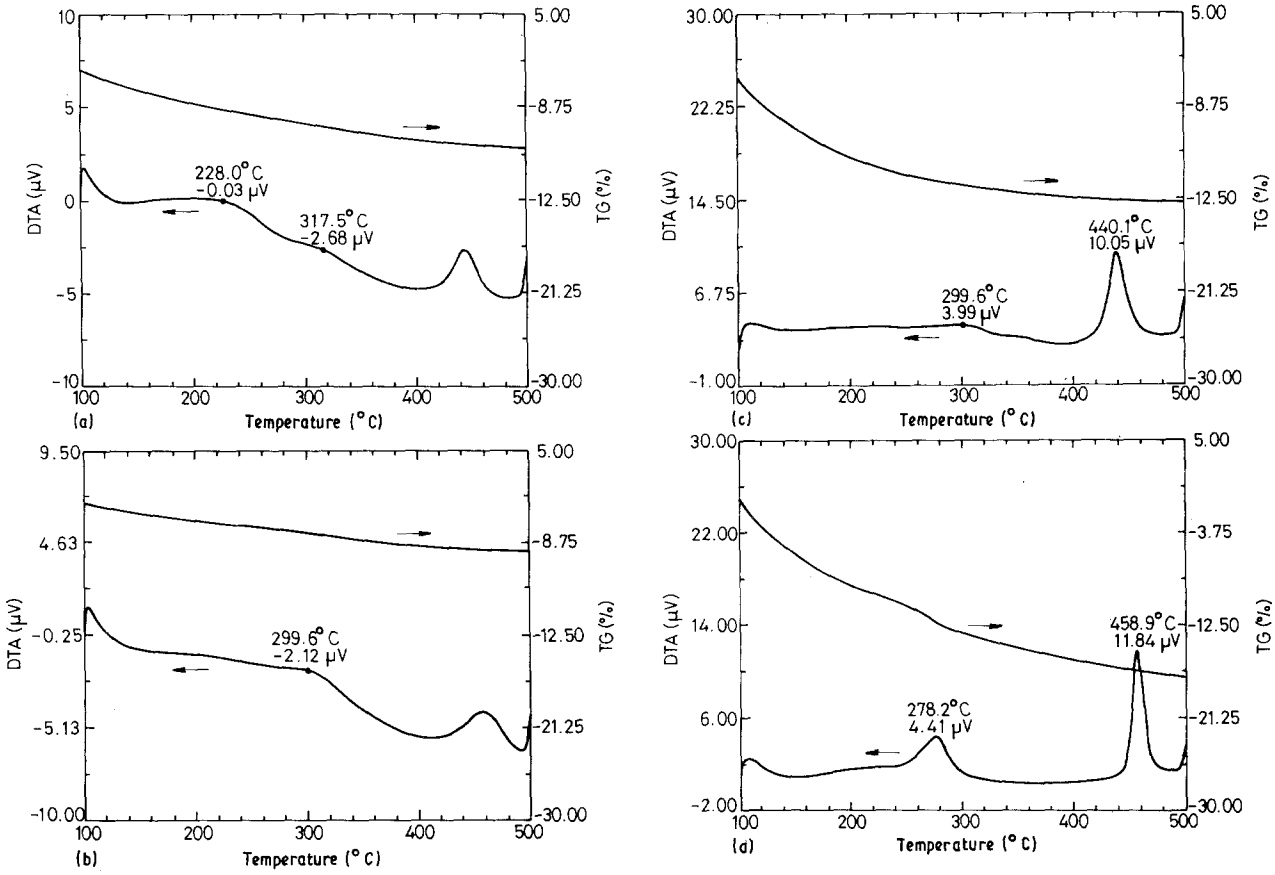

Figure 1 TG/DTA thermograph for 5.3 mol % CeO_2–2 mol % $YO_{1.5}$–ZrO_2 uncalcined powder with various solvent agents: (a) alcohol, (b) acetone, (c) ethyl ether, (d) water.

TABLE I Compositions of powders (x% CeO_2–y% $YO_{1.5}$–ZrO_2) employed in this study

Series	Nominal composition (x–y)	Measured composition (x–y)	Calibrated composition (x–y)
I	5.0–2.0[a]	4.77–1.91	5.00–2.0
	5.2–2.0	5.15–2.00	5.15–2.0
	5.3–2.0	4.97–1.91	5.20–2.0
	5.5–2.0	5.33–1.94	5.50–2.0
	6.0–2.0	5.91–1.97	6.00–2.0
	6.5–2.0	6.37–1.96	6.50–2.0
	8.0–2.0	7.93–1.97	8.05–2.0
	9.0–2.0	8.83–1.93	9.15–2.0
II	6.7–1.5	6.66–1.50	6.66–1.5
	8.7–1.5	8.78–1.50	8.78–1.5
	9.5–1.5	9.21–1.40	9.87–1.5

[a] 5–2 represents 5 mol % CeO_2–2 mol % $YO_{1.5}$–ZrO_2.

TABLE II Surface area and related properties for the synthesized powder

Fabrication process	Alcohol unmilled	Water milled	Alcohol milled
Surface area ($m^2 g^{-1}$)	82.28 ± 0.69	90.67 ± 0.26	106.27 ± 0.54
Particle size[a] (nm)	11.8	10.7	9.1
H_v (GPa)	6.5	6.8	9.0
K_{IC} ($MPa\,m^{1/2}$)	7.3	8.7	16.8
As-sintered density (% TD)	95	96	> 99

[a] Particle size is derived from the equation $D = 6000/\rho A$ based on the ideal sphere model, where D is the corresponding particles size (nm), ρ the theoretical density of the powder ($g\,cm^{-3}$) and A the surface area ($m^2 g^{-1}$).

calibrated composition is the availability to draw the relationship between the composition and the mechanical property, as discussed below.

The powder surface area was analysed by BET with helium as the analysis gas. Table II shows the measured surface area, which casts an influence on the mechanical property. The larger the surface area, the better is the mechanical property and also the denser is the as-sintered bulk. The reason for this is that the large surface area corresponding to fine particles possesses a high driving force for sintering [30]. It appears that the well-fabricated powders by the coprecipitation method are very fine, with a particle size of the order of 10 nm.

The as-fabricated uncalcined powder shows no crystalline phase, as indicated in Fig. 2a. Fig. 2b shows the X-ray diffraction pattern for the calcined powder. There exists an intensive peak around 30° (2θ) which identifies the existence of tetragonal phase. The calcined powders with various compositions employed in this study all exhibit the same results as in Fig. 2b. From the DTA curves as shown in Fig. 1, it can be

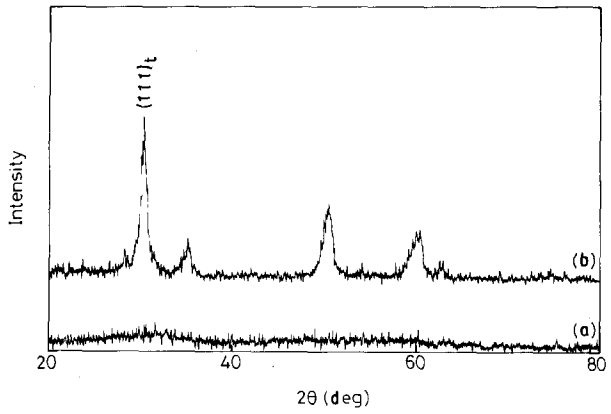

Figure 2 X-ray diffraction patterns of 5.5 mol % CeO_2–2 mol % $YO_{1.5}$–ZrO_2 powder, (a) uncalcined, and (b) calcined at 500 °C for 1 h.

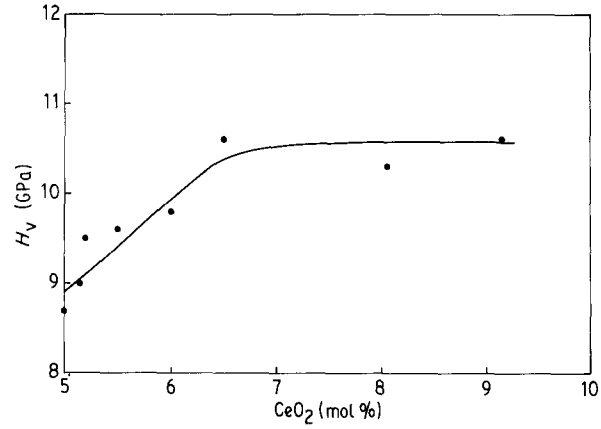

Figure 3 Hardness measurement by the indentation method as a function of CeO_2 content in the 2 mol % $YO_{1.5}$–ZrO_2 system.

concluded that 500 °C is sufficient to calcine the powders in the CeO_2–Y_2O_3–ZrO_2 ceramic system.

3.2. Sintering behaviour

The sintering experiments were carried out at 1500 °C for sintering times ranging from 1–8 h. Table III summarizes the sintering data for the specimen 5.2 mol % CeO_2–2 mol % $YO_{1.5}$–ZrO_2. The average grain size in the as-sintered specimens was estimated by the intercept method. The grain size increases with the sintering time, as expected. The value ranges from 1 μm at 1 h sintering to 2.5 μm at 8 h sintering. Hardness decreases with increasing sintering time due to the increasing grain size. The above observations are in agreement with the previous results reported by Duh *et al.* [20]. It is interesting to note that the fracture toughness is relatively high around a sintering time of 2 h, as indicated in Table III. On the basis of the above descriptions, it appears that the best sintering time at 1500 °C with respect to hardness and fracture toughness is around 2 h in the Ce–Y–TZP ceramic system.

3.3. Mechanical properties

3.3.1. Composition dependence

The mechanical properties of the specimens employed in this study were examined with respect to the hardness and fracture toughness measurement. Fig. 3 shows the relationship between Vickers' hardness and CeO_2 contents in $xCeO_2$–$2YO_{1.5}$–ZrO_2 ceramic system, in which x = 5–9.15 mol %. The hardness increases when CeO_2 contents increase from 5 to 6.5 mol % and then reaches a stable value around 10.6 GPa. The fracture toughness, K_{IC}, calculated from Equation 2, for specimens containing various CeO_2 contents is shown in Fig. 4. Y–TZP containing 5.5 mol % CeO_2 exhibits the highest value of fracture toughness, even exceeding 25 MPa $m^{1/2}$. In fact, the K_{IC} trend in the Ce–Y–TZP system is similar to that in the Y–TZP system [31]. In addition, there appears a wide range of CeO_2 contents, from 5.15–6.5 mol %, which possess K_{IC} over 15 MPa $m^{1/2}$. With respect to both hardness and fracture toughness, the optimum composition is the 5.5 mol % CeO_2–2 mol % $YO_{1.5}$–ZrO_2 ceramic system. Fig. 5 shows scanning

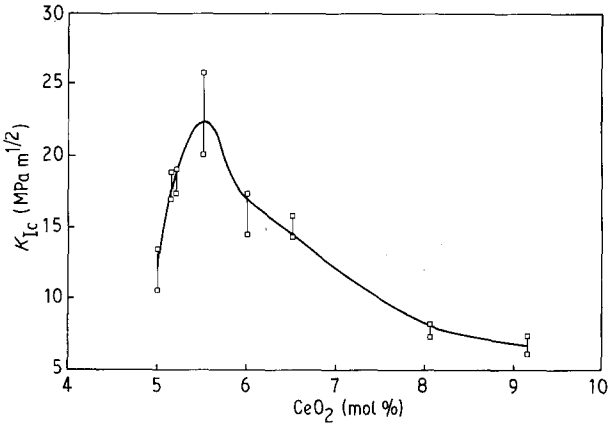

Figure 4 Fracture toughness measurement by the indentation method as a function of CeO_2 content in the 2 mol% $YO_{1.5}$–ZrO_2 system.

TABLE III Sintering data for 5.2 mol % CeO_2–2 mol % $YO_{1.5}$–ZrO_2 at 1500 °C for various periods of time

	Sintering time (h)				
	1	2	4	6	8
Monoclinic phase (%)	13.4	9.6	24.8	22.2	29
Relative density (%)	> 99	98	98	97	98
Grain size (μm)	0.99	1.44	2.03	2.01	2.53
H_v (GPa)	9.2	8.9	8.9	8.8	8.1
K_{IC} (MPa $m^{1/2}$)	18.2 ± 0.4	19.0 ± 1.3	18.1 ± 1.4	16.0 ± 1.0	13.6 ± 2.2

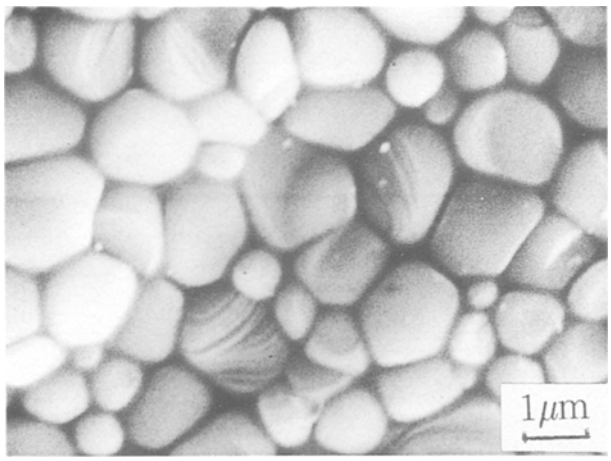

Figure 5 Scanning electron micrographs of the as-sintered surface for the specimen of 5.5 mol % CeO_2–2 mol % $YO_{1.5}$–ZrO_2.

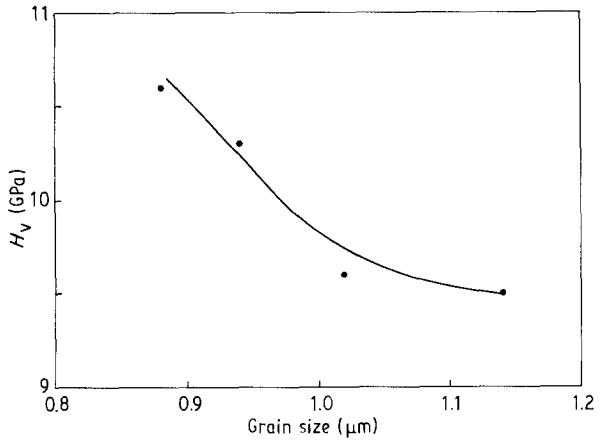

Figure 6 Correlation of hardness values with grain size.

TABLE IV Mechanical data of 1.5 mol % $YO_{1.5}$–ZrO_2 alloyed with various CeO_2 contents

CeO_2 (mol %)	H_v (GPa)	K_{IC} (MPa $m^{1/2}$)	Relative density (%)
6.66	9.1	17.5 ± 0.6	97
8.87	9.7	12.2 ± 0.3	> 99
9.87	> 9.7	6.4 ± 0.1	96

electron micrographs of the as-sintered surface for the specimen 5.5 mol % CeO_2–2 mol % $YO_{1.5}$–ZrO_2. The granular grains exhibit a rather broad size distribution. The smaller ones are in the range of 0.5 μm, while the larger ones are around 2 μm.

Fig. 6 represents the dependence of hardness on the grain size. The hardness decreases with grain size, which is consistent with widely demonstrated variation of hardness with grain size [20]. Deviations from this trend would be due to the effects of density and phase composition. These two are apparently partially related, as expected, possibly because of cracking from the presence of monoclinic phase. Table IV summarizes the mechanical data of CeO_2-doped 1.5 mol % $YO_{1.5}$–ZrO_2 ceramic system. It appears that the hardness in the $x$$CeO_2$–1.5 mol % $YO_{1.5}$–ZrO_2 system is generally lower than that in $x$$CeO_2$–2 mol % $YO_{1.5}$–ZrO_2, due to the lower yttria content. The fracture toughness in the x% CeO_2–1.5% $YO_{1.5}$–ZrO_2 system at $x = 8.87$ is 12.2 MPa $m^{1/2}$. However, Fig. 4 indicates that the K_{IC} value at $x = 8.87$ in the x% CeO_2–2% $YO_{1.5}$–ZrO_2 system is only 7.5 MPa $m^{1/2}$. In addition, it is interesting to note that 6.66 mol % CeO_2–1.5$YO_{1.5}$–ZrO_2 shows lower H_v and higher K_{IC} than 8.87 mol % CeO_2–1.5$YO_{1.5}$–TZP does. Hence, according to Figs 3 and 4, it is expected that there will exist an optimal composition in the $x$$CeO_2$–1.5 mol % $YO_{1.5}$–ZrO_2 ceramic system and that the appropriate CeO_2 composition would lie between 6.66 and 8.87 mol %.

3.3.2. K_{IC} equation evaluation

Equations 2, 4–6 are applied to calculate the fracture toughness measured by the indentation technique. Table V displays the fracture toughness data for specimens with various compositions. As shown in Table V, a lower load (196 N) gives lower l/a value than that under higher load (490 N). Consequently, fracture toughness measured under 196 N load is usually higher than that under 490 N load for $l/a < 2.3$. The effect of indentation load on the fracture toughness in the Ce–Y–TZP system is similar to that in the Y–TZP system [31]. Fig. 7 shows the relationship between fracture toughness and l/a. It appears that all fracture

TABLE V The fracture toughness data for specimens with various compositions

Specimen designation	Load (N)	l/a	K_{IC} (N) Eq. 2	K_{IC} (SWMC) Eq. 4	K_{IC} (L) Eq. 5	K_{IC} (LEM) Eq. 6
5.5–2	490	0.083	25.4 ± 3.5	27.7 ± 3.7	27.1 ± 0.8	13.7 ± 0.4
	490	0.098	23.7 ± 3.4	26.5 ± 3.7	27.0 ± 1.0	13.6 ± 0.5
8.7–1.5	490	0.30	12.2 ± 0.2	13.8 ± 0.3	19.6 ± 0.3	10.0 ± 0.2
6.5–2	490	0.38	11.4 ± 0.8	13.2 ± 0.9	18.5 ± 0.9	9.4 ± 0.5
	196	0.19	12.6 ± 0.9	14.5 ± 0.9	18.7 ± 0.7	9.4 ± 0.4
8–2B	490	1.1	6.9 ± 0.4	8.1 ± 0.5	9.6 ± 0.5	5.0 ± 0.3
	196	0.55	8.0 ± 0.4	9.1 ± 0.1	12.9 ± 0.7	6.6 ± 0.4
8–2A	490	1.5	6.5 ± 0.2	6.7 ± 0.2	9.3 ± 0.5	5.0 ± 0.3
	196	0.62	7.2 ± 0.4	8.0 ± 0.4	11.6 ± 0.7	6.0 ± 0.4
9.5–2	490	2.5	4.5 ± 0.1	5.4 ± 0.1	5.3 ± 0.3	2.8 ± 0.2
	196	1.89	4.3 ± 0.1	5.1 ± 0.1	4.9 ± 0.3	2.6 ± 0.1

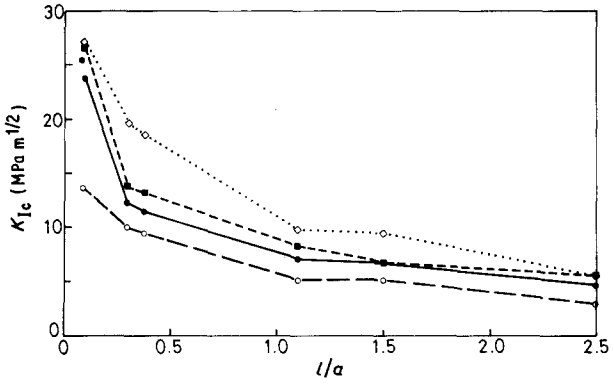

Figure 7 Fracture toughness as a function of l/a. Equation: (—●—) N, (· · ◇ · ·) L, (– – ■ – –) SWMC, (– – ○ – –) LEM.

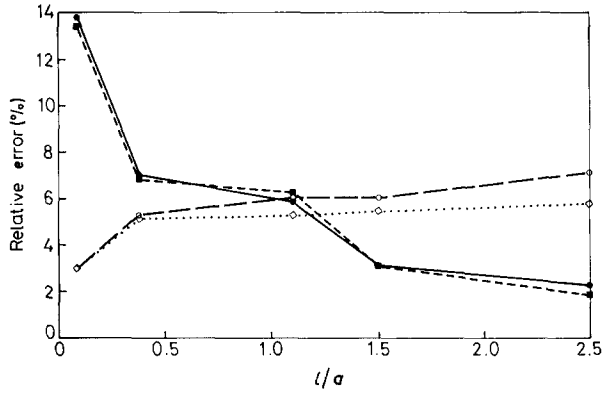

Figure 8 Relationship between relative error and l/a in K_{IC} measurement. Equation: (—●—) N, (· · ◇ · ·) L, (– – ■ – –) SWMC, (– – ○ – –) LEM.

toughnesses calculated using four different equations decrease with increasing l/a. Under the same half-diagonal indent length, a, the shorter surface crack length, l, means higher resistance to crack propagation and hence larger K_{IC} value is observed. In fact, fracture toughness calculated using Equation 5 (L) usually gives the highest value and that computed using Equation 6 (LEM) gives the lowest value, as indicated in Fig. 7. The correlation of relative error, defined as the ratio of deviation to fracture toughness value, as a function of l/a is shown in Fig. 8. In comparison with Equations 5 (L) and 6 (LEM), the larger relative error of Equations 2 (N) and 4 (SWMC) in the low l/a region ($l/a < 0.38$) means that the application of these two equations to low l/a situation, i.e. high K_{IC} value, is improper. However, N and SWMC equations are suitable for use in a high l/a region ($l/a > 1.1$) due to their lower relative error in this region. It should be pointed out that for Equations 5 (L) and 6 (LEM), no l term exists. Thus these two equations are relatively insensitive to l in the low l/a region, where l is critical. On the basis of the above discussions, it is concluded that in the CeO_2–Y_2O_3–ZrO_2 ceramic system both N and SWMC formulations are better ones to apply in the low l/a situation ($l/a < 1.1$), while L and LEM are more suitable to the high l/a region ($l/a > 1.1$). The test load, in fact, presents a considerable factor in fracture toughness measured by the indentation technique.

3.4. Ageing test

The ageing experiments were carried out in 200 °C water for specimens with various compositions for different periods of time. Table VI summarizes the ageing data. As shown in Table VI, the degradation of 5.2–2, 5.5–2 and 6.7–1.5 specimens are obvious after 4 days annealing. This is attributed to the low stabilizer contents to stabilize the tetragonal phase under ageing conditions. Similarly, Specimens 6–2 and 8–2 failed to survive after 7 days and Specimen 8.7–1.5 broke into pieces after ageing for 11 days. However, Specimens 9.5–1.5 and 9–2 retain the same hardness and fracture toughness even after ageing for 21 days.

TABLE VI Hardness and fracture toughness for specimens after different ageing times

Ageing time (days)	Specimen							
	5.2–2	5.5–2	6.7–1.5	6–2	8–2	8.7–1.5	9.5–1.5	9–2
0	9.3[a] / 20.2	9.6 / 22.9	9.1 / 17.5	9.7 / 16.5	10.3 / 7.5	9.9 / 8.2	9.0 / 6.5	10.6 / 6.8
4	[b]	[b]	[b]	9.4 / 14.0	10.4 / 7.3	9.9 / 7.7	[d]	[d]
7				[c]	[c]	10.0 / 7.6	[d]	[d]
11						[c]	[d]	[d]
18							9.0 / 6.5	10.5 / 6.8
21							9.2 / 6.5	10.0 / 6.6

[a] The numerator indicates the hardness, while the denominator presents the fracture toughness.
[b] The specimen broke into pieces during indentor loading.
[c] The specimen broke into pieces after ageing.
[d] No data measured.

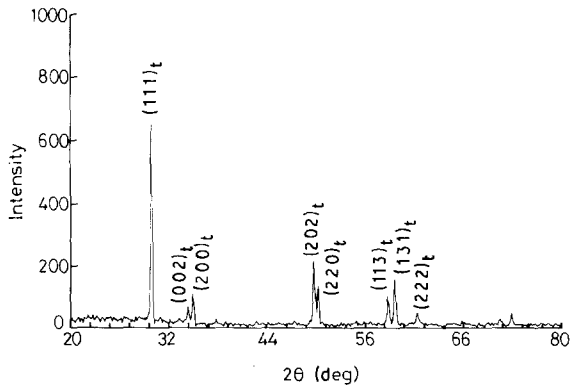

Figure 9 X-ray diffraction patterns for the specimen of 9.5 mol % CeO_2–1.5 mol % $YO_{1.5}$–ZrO_2 after ageing treatment for 21 days.

The X-ray diffraction patterns for Specimen 9.5–1.5 reveal no monoclinic content after ageing treatment, as indicated in Fig. 9. Identical behaviour prevails for Specimen 9–2.

To improve the resistance of Ce–Y–TZP materials to mechanical property degradation on low-temperature ageing, several approaches have been employed through a surface modification technique [32–34]. Continuous research has been conducted in our laboratory by the use of liquid infiltration of cerium-containing solution into Y–TZP ceramics. The results will be reported shortly.

4. Conclusions

1. The coprecipitation process is employed to derive fine powder with various compositions in the CeO_2–Y_2O_3–ZrO_2 ceramic system. Calcination at 500 °C for 1 h is sufficient to achieve full crystallization for derived powders.

2. The mechanical properties of as-sintered specimens are significantly influenced by sintering time. At 1500 °C, the optimum sintering time with respect to hardness and fracture toughness is around 2 h.

3. Vickers' hardness and fracture toughness are measured by the indentation method. The K_{IC} values are affected by the equations employed as well as by the indentor load. The optimum composition for high fracture toughness is 5.5 mol % CeO_2–2 mol % $YO_{1.5}$–ZrO_2 with $K_{IC} > 25\ MPa\,m^{1/2}$ and $H_v \simeq 9.8$ GPa.

4. The ageing degradation decreases with increasing stabilizer content. 2 mol % $YO_{1.5}$–ZrO_2 alloyed with 9 mol % CeO_2 is sufficient to inhibit ageing degradation and 9.5 mol % CeO_2–1.5 mol % $YO_{1.5}$–ZrO_2 ceramic can also endure the ageing treatment.

Acknowledgement

The authors are grateful for the financial support from National Science Council, Taiwan under contract no. NSC80-0405-E-007-12.

References

1. C. T. GRAIN, *J. Amer. Ceram. Soc.* **50** (1967) 288.
2. M. G. SCOTT, *J. Mater. Sci.* **10** (1975) 1527.
3. R. A. MILLER, J. L. SMIALEK and R. G. GARLICK, in "Advances in Ceramics", Vol. 3, "Science and Technology of Zirconia", edited by A. H. Heuer and L. W. Hobbs (The American Ceramic Society, Columbus, OH, 1981) p. 241.
4. J. M. MARDER, T. E. MITCHELL and A. H. HEUER, *Acta Metall.* **31** (1983) 387.
5. D. L. PORTER and A. H. HEUER, *J. Amer. Ceram. Soc.* **62** (1979) 298.
6. T. W. COYLE, W. S. COBLENZ and B. A. BENDER, *Amer. Ceram. Soc. Bull.* **62** (1983) 966.
7. J. G. DUH, H. T. DAI and W. Y. HSU, *J. Mater. Sci.* **23** (1988) 2786.
8. T. K. GUPTA, *Sci. Sintering* **10** (1978) 205.
9. T. K. GUPTA, J. H. BECHTOLD, R. C. KUZNICKIE, L. H. CADOFF and B. R. ROSSING, *J. Mater. Sci.* **12** (1977) 2421.
10. T. K. GUPTA, F. F. LANGE and J. H. BECHTOLD, *ibid.* **13** (1978) 1464.
11. N. CLAUSSEN, M. RUHLE and A. H. HEUER, in "Advances in Ceramics", Vol. 12, "Science and Technology of Zirconia II", edited by N. Claussen (American Ceramic Society, Columbus, OH, 1984) p. 352.
12. F. F. LANGE, *J. Mater. Sci.* **17** (1982) 240.
13. K. KOBAYASHI, H. KUMAJIMA and T. MASAKI, *Solid State Ionics* **3–4** (1981) 489.
14. T. SATO and M. SHIMADA, *J. Amer. Ceram. Soc.* **68** (1985) 356.
15. T. MASAKI, *Int. J. High Tech. Ceram.* **2** (1986) 85.
16. K. TSUKUMA and M. SHIMADA, *J. Mater. Sci. Lett.* **4** (1985) 857.
17. T. SATO, S. OHTAKI, T. ENDO and M. SHIMADA, in "High Tech Ceramics", edited by P. Vincenzini (Elsevier Science, Amsterdam, 1987) p. 281.
18. K. TSUKUMA and M. SHIMADA, *J. Mater. Sci.* **20** (1985) 1178.
19. T. SATO and M. SHIMADA, *Amer. Ceram. Soc. Bull.* **64** (1985) 1382.
20. J. G. DUH, H. T. DAI and B. S. CHIOU, *J. Amer. Ceram. Soc.* **71** (10) (1988) 813.
21. T. SATO, S. OHTAKI, T. ENDO and M. SHIMADA, *Int. J. High Tech. Ceram.* **2** (1986) 167.
22. J. G. DUH and M. Y. LEE, *J. Mater. Sci.* **24** (1989) 4467.
23. H. TORAYA, M. YOSHIMURA and S. SOMIYA, *J. Amer. Ceram. Soc.* **67** (1984) C-119.
24. C. B. PONTON and R. D. RAWLINGS, *Mater. Sci. Technol.* **5** (1989) 856.
25. K. NIIHARA, R. MORENA and D. P. H. HASSELMAN, *J. Mater. Sci. Lett.* **1** (1982) 13.
26. D. K. SHETTY, I. G. WRIGHT, P. N. MINCER and A. H. CLAUER, *J. Mater. Sci.* **20** (1985) 1873.
27. J. LANKFORD, *J. Mater. Sci. Lett.* **1** (1982) 493.
28. B. R. LAWN, A. G. EVANS and D. B. MARSHALL, *J. Amer. Ceram. Soc.* **63** (1980) 574.
29. M. J. TORRALVO and M. A. ALARIO, *J. Catal.* **86** (1984) 470.
30. R. L. COBLE and J. E. BURKE, in "Progress in Ceramic Science", Vol. 3, edited by J. E. Burke (Macmillan, New York, 1966) p. 199.
31. T. MASAKI and K. SHINJO, in "Advanced in Ceramics", Vol. 24B, edited by S. Somiya, N. Yamamoto and N. Yanagida (American Ceramic Society, Columbus, OH, 1988) p. 709.
32. T. SATO, S. OHTAKI, T. FUKUSHIMA, T. ENDO and M. SHIMADA, in "Materials Research Society Symposium Proceedings", Vol. 78. (Materials Research Society, Pittsburgh, PA, USA 1987) p. 147.
33. T. HIOKI, H. HASEGAWA, J. KAWAMOTO and O. KAMIGAITO, in "Advances in Ceramics", Vol. 24B, edited by S. Somiya, N. Yamamoto and H. Yanagida (American Ceramic Society, Columbus, OH, 1988) p. 679.
34. S. J. GLASS and D. J. GREEN, *Adv. Ceram. Mater.* **2** (1987) 129.

Received 16 September
and accepted 27 November 1991